

Experimental determination of superexchange energy from two-hole spectra

Giorgio Levy,^{1,2,*} Maayan Yaari,³ Tom Z. Regier,⁴ and Amit Keren³

¹Quantum Matter Institute, University of British Columbia, Vancouver, British Columbia V6T 1Z4, Canada

²Department of Physics and Astronomy, University of British Columbia, Vancouver, British Columbia V6T 1Z1, Canada

³Department of Physics, Technion - Israel Institute of Technology, Haifa, 3200003, Israel

⁴Canadian Light Source Inc., 44 Innovation Boulevard, Saskatoon, SK, S7N 2V3, Canada

(Dated: July 21, 2021)

We follow the evolution of Copper and Oxygen two-hole excitations, in optimally doped $(\text{Ca}_x\text{La}_{1-x})(\text{Ba}_{1.75-x}\text{La}_{0.25+x})\text{Cu}_3\text{O}_y$ for $x = 0.1$ and $x = 0.4$. The spectra have contributions from band states as well as a localized multiplet structure. From their identification, we determine the intrashell Coulomb interaction U for Oxygen and Copper sites. These results allow us to estimate the atomic superexchange coupling J suggesting a positive correlation between the maximal superconducting critical temperature T_C^{max} and J .

Superconductivity in Copper-based materials (cuprates) emerges from a charge transfer insulator, a state dominated by electronic correlations. In the charge compensated compound $(\text{Ca}_x\text{La}_{1-x})(\text{Ba}_{1.75-x}\text{La}_{0.25+x})\text{Cu}_3\text{O}_y$ (CL123), it arises from an antiferromagnetic phase upon hole doping [1]. It then reaches a maximum critical temperature T_C at a concentration of $p \simeq 0.145$ holes per planar Cu. At a hole concentration $p \sim 0.12$, superconductivity is suppressed and a charge order and pseudogap state appear. However, the charge order and pseudogap energy scales do not seem to be related to superconductivity. In contrast, a comparison of superconducting (SC) and magnetic properties [2] suggests that T_C^{max} grows with increasing superexchange interaction J . This observation was supported by Resonant Inelastic X-ray Scattering (RIXS) [3] and Angle Resolved Photoemission (ARPES) [4] experiments done in the SC phase. The ARPES data was interpreted using the fact that in the Hubbard model $J \sim 100$ meV increases with increasing hopping rate $t \sim 100$ meV [5].

Nevertheless, none of these experiments were completely decisive. Magnetic measurements were done in the non-SC part of the phase diagram and whether their measured trend is extended out to the SC state could be questioned. RIXS suffers from interpretation of the data in terms of J , although the arguments seems to converge with Pärshcke *et al.* [6]. In ARPES, there are two kinds of velocities, below and above the kink in the energy dispersion $E(\mathbf{k})$, where \mathbf{k} is in the (π, π) direction. The Fermi velocity (near zero energy) presents little variation with doping [7–9] or between materials [10] in contrast to the high energy velocity [4]. Which velocity should be compared with T_C is not clear. Moreover, the data depends on surface quality and is noisy when comparing different cleaves even for samples of the same composition. Therefore, a convincing picture can emerge only by performing a variety of different experiments [7] from which the key ingredients guide the models for these materials [11].

The purpose of this study is to evaluate the evolution of the local superexchange interaction J with x in CL123,

and to compare it with $T_C^{\text{max}}(x)$. The structure of CL123 is almost identical to $\text{YBa}_2\text{Cu}_3\text{O}_y$ (Y123) [12], but it is tetragonal with disordered chain layers. The oxygen content y controls the number of doped holes, only slightly affecting the lattice parameters [13]. Doping ranges from magnetic undoped parent compounds to overdoped for all values of x . In contrast, Ca/Ba content x changes only the structural parameters such as bond lengths a , and Cu-O-Cu buckling angles θ , while keeping the net valence fixed [14]. The larger the x , the straighter and tighter is the bond. Disorder in CL123 was found to be x -independent based on the line-widths measured by: high resolution powder x-ray diffraction [15], Cu, Ca, and O nuclear magnetic resonance [16–18], phonon [19], and ARPES [4]. Therefore, disorder is not responsible for variations in T_C^{max} .

Here, we focus on optimally doped single crystals of CL123 from two families: $x=0.1$ and $x=0.4$ where the superconducting transition occurs at 63 and 77 K, respectively. These are the highest critical temperatures achieved for the different x values in a single crystal form. An analysis of the Cu- L_3 and O- K absorption spectra for compositions $x=0.1$ and $x=0.4$ nearly optimally doping shows that both samples have the same amount of holes, which is consistent with previous reports [14, 15]. Then, by combining the previous analysis of the absorption with the electron emission spectra, we determine the energy levels for Cu- d and O- p shells. These values are then used to estimate the superexchange coupling J .

The measurements were performed at the Spherical Grating Monochromator (SGM) beamline located in the Canadian Light Source (CLS) in which the samples were cleaved in a Ultra High Vacuum (UHV) environment better than 5×10^{-9} mbar. To enhance the Auger signal we measure the spectra at the maximum of the absorption line. The X-Ray absorption spectroscopy (XAS) technique was performed in the Total Electron Yield (TEY) mode, where the current needed to compensate for emitted electrons is acquired. The incoming light beam was linearly polarized parallel to the scattering plane defined by the incoming beam and the outgoing electrons. These

were detected using a Hemispherical Scienta analyzer. The samples were oriented with the [001] reciprocal lattice vector perpendicular to the analyzer entrance (in a normal emission configuration) which was also parallel to the normal of the *in situ* cleaved sample surface.

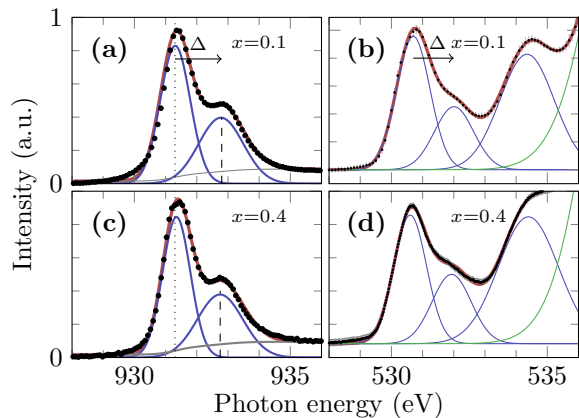


FIG. 1. **Total electron yield as a function of photon energy in CL123** is plotted as black dots. The red curves shows the best fit to the data with a model including Gaussian profiles (blue curves) and a Shirley background plus an offset (black lines). The energy axis for Cu L_3 for $x=0.1$ [(a)] and $x=0.4$ [(c)] compositions were shifted to match the maximum of the spectra near 931.3eV, and the intensity of the main line was normalized to unity. The O K edge for $x=0.1$ is shown in (b) and for $x=0.4$ in (d). The arrows indicate the extracted charge transfer gap value Δ .

Prior to photoemission spectroscopy, we study the doping concentration by x-ray absorption. The absorption spectra of the the spin-orbit split states near the Cu L_3 edge are composed by two lines: a main line at 931.3 eV and a satellite at 932.7 eV [14, 15]. The main is assigned to the transition where a Cu- $2p$ electron is excited to the valence band leaving a core-hole behind. The satellite originates from this transition in the presence of a ligand hole \underline{L} in a molecular orbital formed by the Oxygen atoms surrounding the Copper atom. The main transitions can be represented by $|3d^9\rangle + h\nu \rightarrow |2p, 3d^{10}\rangle$, and the satellite by $|3d^9, \underline{L}\rangle + h\nu \rightarrow |2p, 3d^{10}, \underline{L}\rangle$.

Based on the intensity of the main line and the satellite, the hole concentration can be estimated [15, 20]. In poly-crystalline samples of CL123, the main line barely varies with Calcium content x or Oxygen concentration y [15]. The absorption spectra acquired at the Cu L_3 edge are shown as black dots in Figs. 1(a) and (c) for $x=0.1$ and $x=0.4$ concentrations. The corresponding ones at the Oxygen K edge are shown in Figs. 1(b) and (d), respectively. Following the analysis of Agrestini *et al.* [15], we model the line-shape of the Cu L_3 edge with two Gaussian profiles (blue lines in Fig. 1), a Shirley background (grey line), and an offset. Using the intensities extracted from the fits (red lines in Fig. 1), we can estimate the total amount of holes based on the formula:

$n_h^{L_3} = I_S/(I_M + I_S)$ [20], where $I_S(I_M)$ represents the intensity of the satellite(main) line. We obtain a similar amount of holes $n_h^{L_3} = 0.42 \pm 0.02$ within the error bars for both $x=0.1$ and $x=0.4$ compounds in the optimally doped regime indicating a similar hole concentration.

The doping concentration could also be estimated from an analysis of the Oxygen K (O- K) absorption edge. In the similar compound Y123 [21, 22], this absorption edge consists of a weak pre-edge peak, associated to the O- $2p$ holes on CuO chains followed by a structure at higher photon energies related to the Zhang-Rice state. The following feature at increasing energies has a contribution from final states in the Upper Hubbard Band (UHB). A similar structure is observed within $h\nu=528-533$ eV in CL123 [15], [Fig. 1 (b) and (d)] for both compositions $x=0.1$ and $x=0.4$. In the chosen experimental configuration, the chains barely contribute to the spectra. We therefore relate the feature at 530.7 ± 0.1 eV with a transition involving a ligand hole in the CuO $_2$ planes and the corresponding one at 532 ± 0.1 eV with the UHB [21–23]. The hole concentration can also be estimated from the intensity ratio of these absorption structures. By fitting the absorption spectra with a model containing three Gaussian line-shapes [blue lines in Fig. 1(b) and (d)] plus a high-energy background, the intensity ratio $I_{\underline{L}}/(I_{\underline{L}} + I_{UHB})$ is determined to be 0.60 ± 0.01 , equal within error bars for both compositions.

The charge transfer gap Δ —defined as the energy separation between $3d^9$ and $3d^{10}\underline{L}$ states— can be estimated from the energy difference between the satellite and main line of the Cu- L_3 absorption edge [arrow in Fig. 1(a)]. From the fits to the Cu L_3 spectra discussed before [Fig. 1(a), (c)], we obtain for the $x=0.1$ composition a value of $\Delta_{Cu}^{x01} = 1.6 \pm 0.1$ eV and for $x=0.4$, $\Delta_{Cu}^{x04} = 1.5 \pm 0.1$ eV. The double peak structure appearing in the O- K absorption spectra can also be interpreted as transitions to the charge transfer band at low energies, predominantly of O- $2p$ character— followed by transitions to the UHB dominated by Cu- $3d$ character [24]. The energy separation between these [arrow in Fig. 1(b)] is obtained from the fits to the absorption spectra, $\Delta_O^{x01;x04} = 1.3 \pm 0.1$ eV.

The information extracted so far was obtained by analyzing the internal transitions during the absorption process. To study the electronic correlations, we concentrate on the electron emission spectra that follows the photon absorption. By using the NIST Database [25], we identify the features observed in the photoemission spectra (PES) at photon energies before the absorption edges [see Fig. 2(a)]: the one at a binding energy $BE=-33$ eV with photoemission from La- $5s$ states, at $BE=-27.8$ eV with Ba- $5s$, $BE=-23.5$ eV with O- $2s$, $BE=-20$ eV with Ca- $3p$, $BE=-13.5$ eV with La- $5p$, and $BE=-12.8$ eV with Ba- $5p$. The difference of these features between the $x=0.1$ and $x=0.4$ composition are related to an increase of Ba to Ca concentration with x ; in particular, the intensity decrease at $BE=-27.8$ eV, as well as the

increase around $BE=-20$ eV [Fig. 2(a)].

The PES structure in the region $BE = 0 - 8$ eV is associated with Oxygen and Copper states whose main spectral features are centred around -2 and -4 eV. This assignment is consistent with previous reports on $\text{HgBa}_2\text{Ca}_2\text{Cu}_3\text{O}_{8+\delta}$ [26] and Y123 [27], as well as electronic structure calculations [28]. To better determine their binding energy, we have fit the PES between $BE=1$ eV to $BE=-8$ eV using a model with two Gaussian line-shapes multiplied by a Fermi-Dirac function plus a Shirley background (see Supplemental Materials). From an average of the values obtained with beam energies of $h\nu=528$ and $h\nu=924$ eV, these states are centred at $BE=-1.92\pm 0.04$ eV and $BE=-3.94\pm 0.07$ for the $x=0.1$ composition. For the $x=0.4$ composition, the states are centred at $BE=-1.8\pm 0.1$ and $BE=-3.92\pm 0.04$ eV. From the intensity increase with photon energy of the feature at ~ -2 eV relative to the one at ~ -4 eV [26], as well as their relation with the features in the Auger spectra discussed later, we link the feature at $BE=-3.9\pm 0.1$ eV with O- $2p$ partial Density of States (pDoS) and the corresponding one at $BE=-1.9\pm 0.1$ eV with Cu- $3d$ pDoS.

The electron emission spectra acquired close to the maximum of an absorption edge will include –besides the normal PES– contributions from different decay channels of the excited core-hole. The interference between these channels will mostly be observed in the photon energy evolution of the emission spectra [29, 30] where the excited core-hole has a negligible coupling with the vacuum continuum states. As the photon energy is increased, the wave-function of the excited core-hole starts to overlap significantly with the free-propagating vacuum wave-function, which opens up the emission to Auger electrons. The emitted Auger electrons have a constant kinetic energy independent of the photon energy. In this regime, we can approximate the electron emission as the superposition of the PES and Auger spectra [26, 31].

Within 200 meV of the Cu- L_3 absorption threshold [Fig. 2(b)], the Cu L_3VV Auger transition dominates over the electron photoemission. The acquired spectra is originated from the decay of the core-hole involving Cu- d^{10} excited state into a final Cu- d^8 configuration plus the emission of Auger electrons (ϵ_A). It consists of a broad feature centred around 4 eV plus a triple line structure around 12 eV. The same structure is observed for both $x=0.1$ and $x=0.4$ compositions, albeit a lower relative intensity for the last one. When the beam energy is within 200 meV of the O- K absorption edge [Fig. 2(c)], the photoemission intensity is similar to the Auger component. Notwithstanding, a clear double line contribution around 12 and 15 eV can be observed on the Auger spectra. This component can be extracted by removing the PES acquired at photon energies lower than the absorption edge. This is performed based on the photon energy evolution of the acquired electron emission vs. binding energy spectra [31]. Then, the Auger

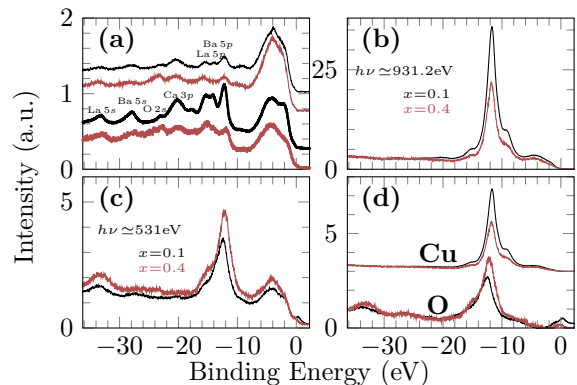


FIG. 2. **Photoemission spectra (PES)** taken around the Cu L_3 and O K absorption edges for compositions $x=0.1$ (in black) and $x=0.4$ (in red). In panel (a), the spectra acquired before the absorption edges for Cu L_3 at $h\nu = 924$ eV (thick lines) and for O K at $h\nu = 528$ eV (thin lines) are shifted vertically for clarity. Close to the absorption edges of Cu L_3 [(b), $h\nu=931$ eV] and O K [(c), $h\nu=531$ eV], the electron emission intensity has normal photoemission and Auger contributions. To extract the Auger component, the PES signal before the absorption edges in (a) is subtracted to the spectra close to the maximum of absorption. The resulted spectra are assigned to the Cu $L_3M_{4,5}M_{4,5}$ [curves shifted vertically upwards in (d)] and to O KL_3L_3 [bottom curves in (d)] transitions. All spectra shown in this Figure have the same intensity normalization.

spectra originated from the core-hole decay involving excited O- $2p^6$ states into a O- $2p^4$ final configuration can be clearly observed. It consists of a broad feature around 7 eV plus a double line structure [bottom curves on Fig. 2(d)] which becomes evident for both $x=0.1$ and $x=0.4$ compositions. The spectra close to the O- K absorption edge also present a structure around $BE \simeq 0$ eV which originate from the attenuated higher harmonics from the synchrotron beam. When the same extraction procedure is applied to the spectra acquired close to the Cu- L_3 edge [top curves on Fig. 2(d)], the broad feature around 4 eV is mostly highlighted. A first inspection at the position of the spectroscopic lines shows that the maximum of the Auger spectra for Cu L_3VV transition is at a lower energy than the corresponding O KVV one. The spectroscopic signatures of the Auger structure are then extracted by fitting the spectra shown in Fig. 2(d) where the broad features are modelled by a Gaussian line-shape, and the multiple lines by Lorentzian ones [see Fig. 3].

The extracted spectroscopic information is interpreted using Cini-Sawatzky theory (CST) [32, 33] as a framework. In this theory, the Auger emission from an atomic closed shell embedded in a solid consists of bound states separated from band states by the intrashell Coulomb repulsion U . Therefore, in the two-hole spectra, the broad feature is assigned to transitions from band states, and the relatively narrower lines to emission from bound state

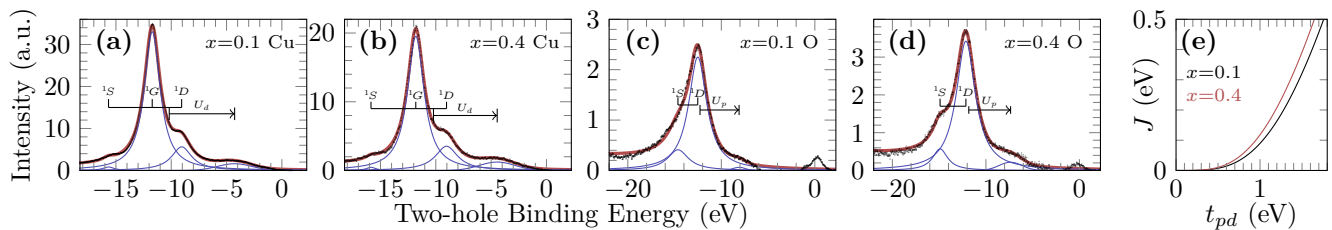


FIG. 3. **The two-hole spectra** is composed of a broad feature representing a continuum followed by a multiplet structure at higher energies. To extract these different components, we have fit the data (black dots) with a model including a Gaussian line-shape and three Lorentzian ones for the resonance close to Cu L_3 edge on $x=0.1$ (a) and $x=0.4$ (b). For the ones close to OK edge, two Lorentzian components are only included for $x=0.1$ (c) and $x=0.4$ (d). Each individual line-shape is shown as a blue curve, and the final model including all the components as a red curve. The energy for the assigned multiplets (1S , 1D , and 1G) and the obtained values for the Coulomb repulsion U (arrows) are shown. From the on-site Coulomb repulsion as well as the charge transfer gap, the variation (e) of the superexchange interaction J with the charge transfer hopping t_{pd} is obtained for $x=0.1$ (black line) and $x=0.4$ (red line).

multiplets. Furthermore, because the direct transition between a spin singlet and triplet configuration of two electrons is forbidden for a spherically symmetric operator – propensity rules [34, 35] – the lines are assigned to final states in the spin-singlet configuration only. For Cu, these would correspond to 1G , 1D , and 1S multiplets and for O, to 1D and 1S . Finally, owing to their spin-singlet configuration, the total spin-orbit coupling for these final states is quenched.

Based on these considerations, we can extract the effective intrashell Coulomb interaction for Cu and O elements from the two-hole spectra. First, the centre and width of the band states are extracted from a fit to the broad features. This assignment is further supported by linking these values with the corresponding pDoS obtained before; the band states are theoretically described by the self-convolution density of states (SCDoS) of the respective pDoS. For $x=0.1$ composition, the band states related to Cu are centred at 4.27 ± 0.03 eV with a full width at half maximum (FWHM) of 3.64 ± 0.06 eV. Second, by associating the lines at increasing two-hole energy with the multiplets $E(^1D)=9.06 \pm 0.01$ eV, $E(^1G)=11.72 \pm 0.01$ eV, and $E(^1S)=15.67 \pm 0.03$ eV, we determine the Slater-Condon parameters [36] (see Supplemental Materials). From them, the effective intrashell Coulomb interaction U is extracted as the difference between the Slater-Condon parameter F^0 and the centre of the band states [37]; which results in $U_d^{x01} \simeq 5.91 \pm 0.03$ eV for $x=0.1$. For $x=0.4$, the band states are centred at 4.45 ± 0.04 eV with a FWHM of 3.8 ± 0.1 eV. From this value and the position of the multiplets, $E(^1D)=9.03 \pm 0.01$ eV, $E(^1G)=11.81 \pm 0.01$ eV, and $E(^1S)=15.86 \pm 0.03$ eV, we obtain $U_d^{x04} \simeq 5.76 \pm 0.04$ eV. In O KVV spectra, the multiplets are located at $E(^1D)=12.52 \pm 0.01$ eV and $E(^1S)=14.64 \pm 0.05$ eV for $x=0.1$ [Fig. 3(c)] composition. An effective O-2p intrashell Coulomb repulsion $U_p^{x01}=4.18 \pm 0.02$ eV relative to the band states is obtained. For $x=0.4$ composi-

tion, the multiplets are located at $E(^1D)=12.14 \pm 0.01$ and $E(^1S)=14.90 \pm 0.03$ eV giving $U_p^{x04}=4.47 \pm 0.06$ eV. Even though the obtained intrashell Coulomb repulsion for Cu-3d states is smaller than the reported values for $\text{Bi}_2\text{CaCu}_2\text{O}_8$ [38] ($U_d \sim 8$ eV), for $\text{La}_{1.85}\text{Sr}_{0.15}\text{CuO}_4$ and $\text{La}_{1.85}\text{Ba}_{0.15}\text{CuO}_4$ [39] ($U_d \simeq 7-8$ eV), it is within the range for the reported value in Y123 [40] ($U_d \simeq 5-7$ eV). Regarding the intrashell Coulomb interaction for O-2p states, our values are similar to the previously reported $U_p \simeq 5$ eV [38–40] in different compounds. This indicates the existence of strong electronic correlations in CL123 similar to other copper-based superconductors.

The atomic antiferromagnetic superexchange coupling J is revealed as one manifestation of the electronic correlations. This coupling would mediate the spin-spin interaction between two adjacent Cu atoms through an intermediate O. Based on a simple atomic transition model [41] which neglects the details of the band-structure [42], we numerically determine the superexchange energy J ; which depends on the Coulomb repulsion between two electrons in O-2p orbitals (U_p), the corresponding one in Cu-3d orbital (U_d), the onsite energy difference Δ_{pd} between them, and the charge transfer hopping t_{pd} (see Supplemental Materials). The trend of J with t_{pd} [Fig. 3(e)], where the other parameters are extracted from the Cu absorption and the two-hole spectra, indicates a higher value for $x=0.4$ than for $x=0.1$ composition. At fixed value of t_{pd} , the increase of the superexchange coupling J is driven by the variation of the Coulomb interaction with x : an increase of the intrashell correlations in O-2p orbitals and a decrease of the ones in Cu-3d. On the other hand, t_{pd} can be estimated from the previously determined values of J [13]: for $x=0.1$, $J=82 \pm 5$ meV and for $x=0.4$, $J=115 \pm 7$ meV; which results in $t_{pd}=0.98 \pm 0.02$ eV and 1.00 ± 0.02 eV, respectively. Thus J increases with x owing mainly to the electronic correlation variations.

In summary, guided by CST and the propensity

rules for Auger transitions, we have identified the band states as well as spin-singlet multiplet excitations of the extracted two-hole spectra of Copper and Oxygen elements on the high- T_C compound $(\text{Ca}_x\text{La}_{1-x})(\text{Ba}_{1.75-x}\text{La}_{0.25+x})\text{Cu}_3\text{O}_y$. Based on their energy, the Coulomb repulsion for electrons in the $O-2p$ (U_p) and $\text{Cu}-3d$ (U_d) states was determined for the compositions $x=0.1$ and $x=0.4$ in the optimally doped regime. Using these values together with the charge-transfer gap extracted from the X-Ray absorption spectra, we have indicated that the atomic superexchange interaction J increases with x as does T_C^{max} . This relation is consistent with the recently reported [43] connection between T_C^{max} and J for different high- T_C families.

Acknowledgments: We thank J. Spalek, A. Nocera, and D. Ellis for useful discussions. This work was performed at the Canadian Light Source, Saskatchewan, Canada. This study was also supported by the Canada First Research Excellence Fund, Quantum Materials and Future Technologies Program; and the Israeli Science Foundation individual grant program 315/17.

* E-mail: levyg@phas.ubc.ca

- [1] M. Bluschke, M. Yaari, E. Schierle, G. Bazalitsky, J. Werner, E. Weschke, and A. Keren, *Phys. Rev. B* **100**, 035129 (2019).
- [2] A. Kanigel, A. Keren, Y. Eckstein, A. Knizhnik, J. S. Lord, and A. Amato, *Phys. Rev. Lett.* **88**, 137003 (2002).
- [3] D. S. Ellis, Y.-B. Huang, P. Olalde-Velasco, M. Dantz, J. Pelliciani, G. Drachuck, R. Ofer, G. Bazalitsky, J. Berger, T. Schmitt, and A. Keren, *Phys. Rev. B* **92**, 104507 (2015).
- [4] G. Drachuck, E. Razzoli, R. Ofer, G. Bazalitsky, R. S. Dhaka, A. Kanigel, M. Shi, and A. Keren, *Phys. Rev. B* **89**, 121119(R) (2014).
- [5] J. Jedrak and J. Spalek, *Phys. Rev. B* **83**, 104512 (2011).
- [6] E. M. Pärshcke, Y. Wang, B. Moritz, T. P. Devereaux, C.-C. Chen, and K. Wohlfeld, *Phys. Rev. B* **99**, 205102 (2019).
- [7] P. V. Bogdanov, A. Lanzara, S. A. Kellar, X. J. Zhou, E. D. Lu, W. J. Zheng, G. Gu, J.-I. Shimoyama, K. Kishio, H. Ikeda, R. Yoshizaki, Z. Hussain, and Z. X. Shen, *Phys. Rev. Lett.* **85**, 2581 (2000).
- [8] X. J. Zhou, T. Yoshida, A. Lanzara, P. V. Bogdanov, S. A. Kellar, K. M. Shen, W. L. Yang, F. Ronning, T. Sasagawa, T. Kakeshita, T. Noda, H. Eisaki, S. Uchida, C. T. Lin, F. Zhou, J. W. Xiong, W. X. Ti, Z. X. Zhao, A. Fujimori, Z. Hussain, and Z.-X. Shen, *Nature* **423**, 398 (2003).
- [9] S. V. Borisenko, A. A. Kordyuk, V. Zabolotnyy, J. Geck, D. Inosov, A. Koitzsch, J. Fink, M. Knupfer, B. Büchner, V. Hinkov, C. T. Lin, B. Keimer, T. Wolf, S. G. Chiuzbaian, L. Patthey, and R. Follath, *Phys. Rev. Lett.* **96**, 117004 (2006).
- [10] B. Edegger, V. N. Muthukumar, C. Gros, and P. W. Anderson, *Phys. Rev. Lett.* **96**, 207002 (2006).
- [11] J. Spalek, M. Zegrodnik, and J. Kaczmarczyk, *Phys. Rev. B* **95**, 024506 (2017).
- [12] D. Goldschmidt, G. M. Reisner, Y. Direktovitch, A. Knizhnik, E. Gartstein, G. Kimmel, and Y. Eckstein, *Phys. Rev. B* **48**, 532 (1993).
- [13] R. Ofer, G. Bazalitsky, A. Kanigel, A. Keren, A. Auerbach, J. S. Lord, and A. Amato, *Phys. Rev. B* **74**, 220508(R) (2006).
- [14] S. Sanna, S. Agrestini, K. Zheng, R. D. Renzi, and N. L. Saini, *EPL* **86**, 67007 (2009).
- [15] S. Agrestini, S. Sanna, K. Zheng, R. De Renzi, E. Pusceddu, G. Concas, N. L. Saini, and A. Bianconi, *Journal of Physics and Chemistry of Solids* **75**, 259 (2014).
- [16] A. Keren, *New Journal of Physics* **11**, 065006 (2009).
- [17] E. Amit and A. Keren, *Phys. Rev. B* **82**, 172509 (2010).
- [18] T. Cvitančić, D. Pelc, M. Požek, E. Amit, and A. Keren, *Phys. Rev. B* **90**, 054508 (2014).
- [19] D. Wulferding, M. Shay, G. Drachuck, R. Ofer, G. Bazalitsky, Z. Salman, P. Lemmens, and A. Keren, *Phys. Rev. B* **90**, 104511 (2014).
- [20] N. Merrien, L. Coudrier, C. Martin, A. Maignan, F. Studer, and A. M. Flank, *Phys. Rev. B* **49**, 9906 (1994).
- [21] N. Nucker, E. Pellegrin, P. Schweiss, J. Fink, S. L. Molodtsov, C. T. Simmons, G. Kaindl, W. Frentrup, A. Erb, and G. Muller-Vogt, *Phys. Rev. B* **51**, 8529 (1995).
- [22] D. G. Hawthorn, K. M. Shen, J. Geck, D. C. Peets, H. Wadati, J. Okamoto, S.-W. Huang, D. J. Huang, H.-J. Lin, J. D. Denlinger, R. Liang, D. A. Bonn, W. N. Hardy, and G. A. Sawatzky, *Phys. Rev. B* **84**, 075125 (2011).
- [23] M. Merz, N. Nucker, P. Schweiss, S. Schuppler, C. T. Chen, V. Chakarian, J. Freeland, Y. U. Idzerda, M. Klaser, G. Muller-Vogt, and T. Wolf, *Phys. Rev. Lett.* **80**, 5192 (1998).
- [24] C. T. Chen, F. Sette, Y. Ma, M. S. Hybertsen, E. B. Stechel, W. M. C. Foulkes, M. Schluter, S.-W. Cheong, A. S. Cooper, L. W. Rupp, B. Batlogg, Y. L. Soo, Z. H. Ming, A. Krol, and Y. H. Kao, *Phys. Rev. Lett.* **66**, 104 (1991).
- [25] N. Database, *NIST X-Ray Photoelectron Spectroscopy Database, standard reference database number 20* (2020).
- [26] A. Chainani, M. Sicot, Y. Fagot-Revurat, G. Vasseur, J. Granet, B. Kierren, L. Moreau, M. Oura, A. Yamamoto, Y. Tokura, and D. Malterre, *Phys. Rev. Lett.* **119**, 057001 (2017).
- [27] A. Balzarotti, M. De Crescenzi, N. Motta, F. Patella, and A. Sgarlata, *Phys. Rev. B* **38**, 6461 (1988).
- [28] W. E. Pickett, *Rev. Mod. Phys.* **61**, 433 (1989).
- [29] F. Gel'mukhanov and H. Ågren, *Physics Reports* **312**, 87 (1999).
- [30] G. Levy, R. Sutarto, D. Chevrier, T. Regier, R. Blyth, J. Geck, S. Wurmehl, L. Harnagea, H. Wadati, T. Mizokawa, I. S. Elfimov, A. Damascelli, and G. A. Sawatzky, *Phys. Rev. Lett.* **109**, 077001 (2012).
- [31] R. Kraus, V. Bisogni, L. Harnagea, S. Aswartham, S. Wurmehl, G. Levy, I. S. Elfimov, B. Büchner, G. A. Sawatzky, and J. Geck, *Phys. Rev. B* **87**, 134516 (2013).
- [32] M. Cini, *Solid State Communications* **24**, 681 (1977).
- [33] G. A. Sawatzky, *Phys. Rev. Lett.* **39**, 504 (1977).
- [34] H. Ågren and O. Vahtras, *J. Phys. B: At. Mol. Opt. Phys.* **26**, 913 (1993), publisher: IOP Publishing.
- [35] A. Kyiene and R. Karazija, *Phys. Scr.* **70**, 288 (2004).
- [36] J. Griffith, *The theory of transition-metal ions* (Cam-

- bridge University Press, 1961).
- [37] G. A. Sawatzky and A. Lenselink, *Phys. Rev. B* **21**, 1790 (1980).
- [38] L. H. Tjeng, C. T. Chen, and S.-W. Cheong, *Phys. Rev. B* **45**, 8205 (1992).
- [39] R. Bar-Deroma, J. Felsteiner, R. Brener, J. Ashkenazi, and D. van der Marel, *Phys. Rev. B* **45**, 2361 (1992).
- [40] D. van der Marel, J. van Elp, G. A. Sawatzky, and D. Heitmann, *Phys. Rev. B* **37**, 5136 (1988).
- [41] E. Pavarini, E. Koch, R. Scalettar, and R. Martin, eds., *The Physics of Correlated Insulators, Metals, and Superconductors*, Schriften des Forschungszentrums Jülich Reihe Modeling and Simulation, Vol. 7 (Forschungszentrum Jülich GmbH Zentralbibliothek, Verlag, Jülich, 2017) p. 450 p.
- [42] H. Eskes and J. H. Jefferson, *Phys. Rev. B* **48**, 9788 (1993).
- [43] L. Wang, G. He, Z. Yang, M. Garcia-Fernandez, A. Nag, K.-J. Zhou, M. Minola, M. L. Tacon, B. Keimer, Y. Peng, and Y. Li, [arXiv:2011.05029 \[cond-mat\]](https://arxiv.org/abs/2011.05029) (2020), arXiv:2011.05029.